Analysis of Vibrational Raman Optical Activity Signatures of the $(TG)_N$ and $(GG)_N$ Conformations of Isotactic Polypropylene Chains in Terms of Localized Modes

Vincent Liégeois,*,†,‡ Christoph R. Jacob,¶,‡ Benoît Champagne,† and Markus Reiher*,‡

Laboratoire de Chimie Théorique, Groupe de Chimie Physique, Facultés Universitaires Notre-Dame de la Paix, rue de Bruxelles, 61, B-5000 Namur, Belgium, Laboratorium für Physikalische Chemie, ETH Zürich, Wolfgang-Pauli-Str. 10, CH-8093 Zürich, Switzerland, and Center for Functional Nanostructures, Karlsruhe Institute of Technology (KIT), Wolfgang-Gaede-Str. 1a, 76131 Karlsruhe, Germany

Received: March 26, 2010; Revised Manuscript Received: May 18, 2010

In a previous study [Lamparska, E.; Liégeois, V.; Quinet, O.; Champagne, B. *ChemPhysChem* **2006**, *7*, 2366−2376], signatures associated to the helical structure of a small oligomer of a polypropylene chain were highlighted in the vibrational Raman optical activity (VROA) spectra. Nevertheless, it was difficult to pursue the analysis of longer chains. Indeed, the number of normal modes is becoming large and they are delocalized over the whole chain, increasing the complexity of their analysis. With a new tool developed to analyze the vibrational spectra [Jacob, Ch. R.; Reiher, M. *J. Chem. Phys.* **2009**, *130*, 084106], one can understand the normal modes, the VROA intensity of the bands, and the band shapes of long polymer chains by investigating the vibrational coupling matrices and the intensity coupling matrices. The VROA couplet at around 1100 cm^{-1} (previously evidenced as a signature of the $(TG)_N$ helical pitch) can now be thoroughly analyzed and compared to the corresponding signature in the $(GG)_N$ conformer. The mode localization approach shows that for both conformations this couplet arises from a phase difference within the localized modes of both peaks, leading to the inversion of the sign of the total VROA intensity. Comparing the $(TG)_N$ and $(GG)_N$ conformers, the vibrational and intensity coupling matrices completely change with the modification of the structure. This leads for the $(TG)_{19}$ conformer to a negative-positive couplet, whereas for the $(GG)_{19}$ conformation, a characteristic positive-negative-positive pattern is found.

1. Introduction

The determination of the structure of polymer chains is crucial in order to understand the properties of polymeric materials. These materials consist of long flexible chains that intermingle with each others. Therefore, the study of the conformations—or conformational distributions—of these chains is of primary importance. Among the available techniques, Raman spectroscopy has demonstrated its specificity.[1,2] For instance, it is employed for unravelling local and collective motions,[3] conformational disorder,[4] chemical doping,[5] and chain packing.[6] Compared to IR spectroscopy, Raman spectroscopy is very sensitive to conformational aspects, and it is little affected by solvent interferences.

Especially vibrational Raman optical activity (VROA) spectroscopy[7−9] is a powerful technique to study configurations as well as conformations of molecules,[8,10−22] macromolecules of the living world,[23−31] and synthetic polymers.[32−36] In particular, specific signatures of characteristic conformations such as α-helices and β-sheets,[23,24,30,31] or helical pitches,[32,34−36] have been highlighted in these studies. A challenge for VROA spectroscopy is to provide a catalogue of rules-of-thumbs that could be used to interpret dominant spectral signatures, just as it has been accomplished for IR and Raman spectroscopy.

Some first attempts to investigate VROA fingerprints of helical conformations of synthetic polymers were conducted earlier.[33−35] In particular, the Raman and VROA spectra of a small 3-unit isotactic polypropylene chain were analyzed[35] as a model for a longer polymeric backbone. Such carbon backbones can adopt mostly four different regular conformation: $(TT)_N$, $(TG)_N$, $(GG)_N$, and $(TGTG')_N$ where T means 180° (trans) torsion angle, and G and G′ stand for 60° and −60° (gauche) torsion angles, respectively. The first conformation, which is the thermodynamically preferred one for a syndiotactic polypropylene chain, has a mirror plane and therefore no VROA intensity. The $(TG)_N$ and its enantiomeric $(TG')_N$ conformations lead to a 3-fold helicity and are the thermodynamically favored conformations for an isotactic polypropylene chain. The $(GG)_N$ conformation exhibits a 4-fold helicity whereas the $(TGTG')_N$ one has no screw axis. The conclusion of ref 35 was that VROA is more sensitive than Raman spectroscopy to discriminate between the different helical patterns. Moreover, a couplet at around 1100 cm^{-1} was evidenced as a specific signature for the $(TG)_N$ conformation.

However, this preliminary work was done on a small oligomer and confirmation on longer chains was always in the perspective. Nevertheless, investigations on longer chains are not only more computer time-consuming but also more challenging to analyze since the number of normal modes increases while they are delocalized over the whole chain. However, a new tool to analyze the normal modes of vibration and the Raman/VROA intensities has been recently developed.[37] It localizes the vibrational normal modes through a unitary transformation of the normal modes of one specific VROA band. From this, the total band intensity as well as the coupling between the localized modes that give rise to the band shape can be analyzed. The first applications of this method[38,39] focused on α-helix and 3_{10}-

* To whom correspondence should be addressed: E-mail: vincent.liegeois@fundp.ac.be; markus.reiher@phys.chem.ethz.ch.
† Facultés Universitaires Notre-Dame de la Paix.
‡ ETH Zürich.
¶ Karlsruhe Institute of Technology.

10.1021/jp102739g
Published on Web 06/14/2010

helix conformations of a polypeptide containing 20 (*S*)-alanine residues. In particular, different vibrational and intensity coupling patterns were evidenced between the two types of helices in relation with the structural changes between both structures.

The purpose of the present work is to investigate the difference of signatures between the 3-fold $(TG)_N$ and 4-fold $(GG)_N$ conformations for isotactic polypropylene chain of relatively long size (20 units). In this study, employing the mode localization approach, we particularly focus on the couplet at around 1100 cm^{-1} that was described as a signature of the $(TG)_N$ conformation of the 3-unit chain:[35] (i) in order to assess whether this signature is conserved while elongating the chain as well as (ii) to confirm that the signature is associated with the $(TG)_N$ conformation and therefore that the $(GG)_N$ conformation exhibit another pattern. The mode localization method, only used for polypeptides until now, is particularly useful to analyze delocalized normal modes of a given band and is going to provide informations about the impact of the modification of the structure between both conformations.

Our attempt to better understand the vibrational spectra of polymers is a continuation of previous studies.[40−44] In these papers, some methods to calculate vibrational spectra by using explicitly the translation or the screw operators have been developed and applied. One method[42] consists in calculating the force-constant matrix, expressed in Cartesian coordinates, between the different units of the chain. In our contribution, we consider a similar quantity, namely the vibrational coupling matrix $\tilde{\mathbf{\Omega}}$ but expressed in terms of localized modes of one band. The different normal modes within one band can be associated to discrete values of **k**, the phonon wavenumber.

The article is divided into seven parts. Section 2 reviews the theoretical aspects of simulating a VROA spectrum. The analysis in terms of localized modes is explained in Section 3. The computational aspects are provided in Section 4. The VROA signatures for both conformations are detailed in Section 5. They are subsequently analyzed in terms of the total band intensities and the band shapes in Sections 6 and 7, respectively. Conclusions are drawn in Section 8.

2. VROA Theory

The vibrational Raman optical activity (VROA) spectroscopy measures the tiny difference in Raman scattering between right- and left-handed incident circularly polarized light (ICP scheme). In the measurement, the time-averaged power of the photons scattered within a cone of solid angle $d\Omega$, called radiant intensity I (Js^{-1} sr^{-1}), is recorded. This intensity is proportional to the time-averaged energy flux of the incident beam, called irradiance $\mathcal{I}$ (Js^{-1} m^{-2}): $I = (d\sigma)/(d\Omega).\mathcal{I}$, where the factor of proportionality is called the differential scattering cross section (m^2/sr) and is the quantity calculated by ab initio methods. Within the harmonic approximation, the differential VROA scattering cross section for a naturally polarized incident light (n) in the scattered circularly polarized (SCP) scheme for a scattering angle θ and the pth vibrational normal mode reads:[7−9]

$$-\Delta^{n}d\sigma(\theta)_{SCP,p} = \frac{2K_p}{c}\langle 1_p|Q_p|0_p\rangle^2[45aG'^2_p + 13\beta^2_{Gp} - \beta^2_{Ap} + \cos(\theta)(90aG'^2_p - 10\beta^2_{Gp} - 6\beta^2_{Ap}) + \cos^2(\theta)(45aG'^2_p + \beta^2_{Gp} + 3\beta^2_{Ap})]d\Omega \quad (1)$$

To express σ in m^2 (SI units are used throughout the paper), the constant K_p is given by:

$$K_p = \frac{1}{90}\left(\frac{\mu_0}{4\pi}\right)^2\omega_p^3\omega_0 \quad (2)$$

where $\omega_0 = 2\pi\nu_0$ is the angular frequency of the laser beam, ω_p is the angular frequency of the scattered light, and μ_0 is the permeability constant. In the harmonic approximation, for a fundamental vibrational transition ($1_p \leftarrow 0_p$):

$$\langle 1_p|Q_p|0_p\rangle^2 = \hbar/(2\Delta\omega_p) \quad (3)$$

where $\Delta\omega_p$ corresponds to the vibrational transition associated with the normal coordinate Q_p. In the specific case of a backward-scattering ($\theta = \pi$) setup, which is considered in the following simulations, eq 1 then reads:

$$-\Delta^{n}d\sigma(\pi)_{SCP,p} = \frac{1}{90}\frac{1}{c^4}\omega_p^3\omega_0\frac{\hbar}{2\Delta\omega_p}\underbrace{\frac{1}{c16\pi^2\varepsilon_0^2}[48\beta^2_{Gp} + 16\beta^2_{Ap}]}_{m^4Kg^{-1}}d\Omega\ [m^2/sr] \quad (4)$$

where the underbrace quantity is often referred to as the VROA intensity expressed in $Å^4$/amu (SI units: m^4 kg^{-1}). These units are obtained while using polarizability volumes,[45] that is, the polarizability divided by $4\pi\varepsilon_0$. In the following, intensities given in $Å^4$/amu will refer to the underbrace quantity instead of the total intensity given by eq 4. The main difference is that the intensity given in $Å^4$/amu does not depend anymore on the vibrational frequency $\Delta\omega_p$.

The three invariants in eq 1 (aG'_p, β^2_{Gp}, and β^2_{Ap}) require the evaluation of the first-order derivatives of three polarizability tensors: $(\partial\alpha/\partial Q_p)$, $(\partial A/\partial Q_p)$ and $(\partial G'/\partial Q_p)$. A review by Buckingham[46] defines all these polarizabilities. The invariants have then the form:

$$aG'_p = \frac{1}{9}\sum_{\mu,\nu}\left(\frac{\partial\alpha_{\mu\mu}}{\partial Q_p}\right)_0\left(\frac{\partial G'_{\nu\nu}}{\partial Q_p}\right)_0 \quad (5)$$

$$\beta^2_{Gp} = \frac{1}{2}\sum_{\mu,\nu}\left[3\left(\frac{\partial\alpha_{\mu\nu}}{\partial Q_p}\right)_0\left(\frac{\partial G'_{\mu\nu}}{\partial Q_p}\right)_0 - \left(\frac{\partial\alpha_{\mu\mu}}{\partial Q_p}\right)_0\left(\frac{\partial G'_{\nu\nu}}{\partial Q_p}\right)_0\right] \quad (6)$$

$$\beta^2_{Ap} = \frac{\omega_0}{2}\sum_{\mu,\nu}\sum_{\lambda,\kappa}\left[\left(\frac{\partial\alpha_{\mu\nu}}{\partial Q_p}\right)_0\left(\frac{\varepsilon_{\mu\lambda\kappa}\partial A_{\lambda\kappa\nu}}{\partial Q_p}\right)_0\right] \quad (7)$$

In the above summations, the indices μ, ν, λ, and κ are components of the electric or magnetic fields (x, y, z). $\varepsilon_{\mu\lambda\kappa}$ is the antisymmetric unit tensor of Levi-Civita. The subscript 0 indicates that the properties are evaluated at the equilibrium geometry.

3. Localization of Normal Modes

To analyze the vibrational spectra of large molecules, a new tool has recently been developed.[37] It consists of performing a unitary transformation on a subset of k normal modes ($\mathbf{Q}^{sub}$) belonging to a specific band in order to obtain localized modes,

$$\tilde{\mathbf{Q}}^{sub} = \mathbf{Q}^{sub}\mathbf{U} \quad (8)$$

where the unitary transformation $\mathbf{U}$ is chosen in such a way that it yields to the "most localized" modes $\tilde{\mathbf{Q}}^{\mathrm{sub}}$. Note that throughout this paper, a tilde is used on all quantities that refer to localized modes instead of vibrational normal modes. Possible criteria to achieve this are described in details in ref 37, but their explicit choice hardly affects the form of the localized modes produced. Here, we employed the atomic-contribution ξ_{at} criterion introduced in ref 37.

The vibrational normal modes constitute a basis in which the mass-weighted Hessian, $H^m_{i\alpha,j\beta} = (1/(m_i m_j)^{1/2})(\partial^2 E/\partial R_{i\alpha}\partial R_{j\beta})_0$, is diagonal:

$$\mathbf{Q}^T\mathbf{H}^m\mathbf{Q} = \mathbf{H}^q \tag{9}$$

where $\mathbf{H}^q$ is a diagonal matrix with the individual elements equal to the squares of the angular frequencies, $H^q_{pp} = \omega_p^2 = 4\pi^2\nu_{\mathrm{p}}^2$, with ν_{p} being the pth vibrational frequency. The pth column of the unitary matrix $\mathbf{Q}$, denoted $\mathbf{Q}_p$, is the pth normal mode in terms of mass-weighted Cartesian coordinates. The components of this mode in terms of Cartesian coordinates $\mathbf{Q}^c_p$ is then expressed as $Q^c_{i\alpha,p} = (1/\sqrt{m_i})Q_{i\alpha,p}$. In the matrix terms, the indices i and j denote atomic nuclei while α and β are used for Cartesian components (x, y, z).

In the basis of the localized modes, the mass-weighed Hessian is not longer diagonal:

$$\tilde{\mathbf{Q}}^{T,\mathrm{sub}}\mathbf{H}^{m,\mathrm{sub}}\tilde{\mathbf{Q}}^{\mathrm{sub}} = \tilde{\mathbf{H}}^{\mathrm{sub}} = \mathbf{U}^T\mathbf{H}^{q,\mathrm{sub}}\mathbf{U} \tag{10}$$

The diagonal elements of the matrix $\tilde{\mathbf{H}}^{\mathrm{sub}}$ are squares of the fictitious angular frequencies $\tilde{H}^{\mathrm{sub}}_{pp} = \tilde{\omega}_p^2 = 4\pi^2\tilde{\nu}_p^2$ of the localized modes while the off-diagonal elements $\tilde{H}^{\mathrm{sub}}_{pq}$ can be interpreted as coupling between localized modes p and q. However, the numerical values of the couplings are not easy to analyze as they refer to squares of angular frequencies instead of vibrational frequencies. Therefore, it is useful to introduce a new quantity, the vibrational coupling matrix $\tilde{\mathbf{\Omega}}$, defined as:[37]

$$\tilde{\mathbf{\Omega}} = \mathbf{U}^T\mathbf{\Omega}\mathbf{U} \tag{11}$$

where $\mathbf{\Omega}$ is the diagonal matrix with $\mathbf{\Omega}_{pp} = \bar{\nu}_p = \omega_p/(2\pi c)$, the wavenumbers of the vibrational normal modes.

The main advantage of the localized modes over the normal modes, which are usually delocalized over a whole chain of identical subunits, is that they only involve the displacement of few atoms centered at one of the units in the chain. Moreover, for a regular chain, the different localized modes involve similar atomic displacements but are located on different units of the chain. It is therefore all the different in-phase and out-of-phase combinations (produced by the $\mathbf{U}$ matrix) of the localized mode that yield to delocalized vibrational normal modes.

The coupling matrix $\tilde{\mathbf{\Omega}}$ defined earlier provides an useful tool to analyze the position of the peaks within a given band. The localized modes (and the unitary transformation matrix) can also be applied to understand the total band intensities and shapes (i.e., how the intensity of a band is spread over all the normal modes). For this purpose, one defines an intensity coupling matrix $\tilde{\mathbf{I}}$ from the following transformation:[37]

$$I_p = \sum_{qr} U_{pq}U_{pr}\tilde{I}_{qr} \tag{12}$$

where I_p is the intensity of the pth normal mode. The diagonal elements of this matrix, $\tilde{I}_{qq}$, are referred to as intensity of the qth localized modes, and the off-diagonal values, $\tilde{I}_{qr}$, are the intensity coupling terms. An shown in ref 37, the total intensity of the considered band $\Sigma_p I_p$ is equal to the sum of the intensity of the localized modes, $\Sigma_q \tilde{I}_{qq}$. Since the atomic displacements of the localized modes are usually similar, so are their intensities. The total intensity of the band can therefore be investigated simply by analyzing the intensity of one localized mode. For the band shape, the intensity coupling matrix $\tilde{\mathbf{I}}$ together with the transformation matrix $\mathbf{U}$ (eigenvectors of $\tilde{\mathbf{\Omega}}$) describes how the intensities of the localized modes are distributed in the vibrational normal modes.

To analyze the VROA intensity of a normal mode or of a localized mode, we use the decomposition scheme called group coupling matrix (GCM) introduced by Hug:[47]

$$I_p = \sum_{i,j}^{N}\sum_{\alpha,\beta}^{3} Q^c_{i\alpha,p}V_{i\alpha,j\beta}Q^c_{j\beta,p} = \sum_{i,j} I_{ij,p} \tag{13}$$

$$\tilde{I}_q = \sum_{i,j}^{N}\sum_{\alpha,\beta}^{3} \tilde{Q}^c_{i\alpha,q}V_{i\alpha,j\beta}\tilde{Q}^c_{j\beta,q} = \sum_{i,j} \tilde{I}_{ij,q} \tag{14}$$

where $V_{i\alpha,j\beta} = (1/c16\pi^2\varepsilon_0^2)[48V(\beta^2_{\mathrm{G}})_{i\alpha,j\beta} + 16V(\beta^2_{\mathrm{A}})_{i\alpha,j\beta}]$ is the linear combination of the VROA invariants, which are functions of the Cartesian derivatives of the three polarizabilities:

$$V(\beta^2_{\mathrm{G}})_{i\alpha,j\beta} = \frac{1}{2}\sum_{\mu,\nu}\left[3\left(\frac{\partial\alpha_{\mu\nu}}{\partial R_{i\alpha}}\right)_0\left(\frac{\partial G'_{\mu\nu}}{\partial R_{j\beta}}\right)_0 - \left(\frac{\partial\alpha_{\mu\mu}}{\partial R_{i\alpha}}\right)_0\left(\frac{\partial G'_{\nu\nu}}{\partial R_{j\beta}}\right)_0\right] \tag{15}$$

$$V(\beta^2_{\mathrm{A}})_{i\alpha,j\beta} = \frac{\omega_0}{2}\sum_{\mu,\nu}\sum_{\lambda,\kappa}\left[\left(\frac{\partial\alpha_{\mu\nu}}{\partial R_{i\alpha}}\right)_0\left(\frac{\varepsilon_{\mu\lambda\kappa}\partial A_{\lambda\kappa\nu}}{\partial R_{j\beta}}\right)_0\right] \tag{16}$$

Using the previous summations, eqs 13 and 14, the VROA intensity for a given normal or localized mode p can be decomposed into homonuclear ($I_{ii,p}$) and heteronuclear ($I_{ij,p}$) contributions. Then, using straightforward summations, these definitions can be generalized to groups of atoms. The diagonal terms are mononuclear or intragroup, and the off-diagonal terms are dinuclear or intergroup, respectively. As only the symmetric part contributes to the total intensity of the vibrational modes, they are best represented by upper triangular matrices, with off-diagonal elements equal to the sum of the two off-diagonal halves of the full matrix. In the GCM scheme of Hug, the matrix elements are visualized as circles, with an area proportional to the $I_{ij,p}$ (or $\tilde{I}_{ij,p}$) values, whereas their color is related to their sign. The factor of proportionality is tunable but fixed throughout this work for consistency of their analysis.

4. Computational Methodology

The initial structures of the $(TG)_{19}$ and $(GG)_{19}$ conformations of the isotactic polypropylene chain have been constructed with the ideal torsion angles. The optimizations of these structures were then performed with the TURBOMOLE program[48,49] employing density-functional theory (DFT) with the BP86 exchange-correlation functional[50,51] and Ahlrichs' valence triple-ζ basis with one set of polarization functions (TZVP).[52]

The vibrational frequencies and vibrational normal modes as well as the atomic Cartesian derivatives of the three polariz-

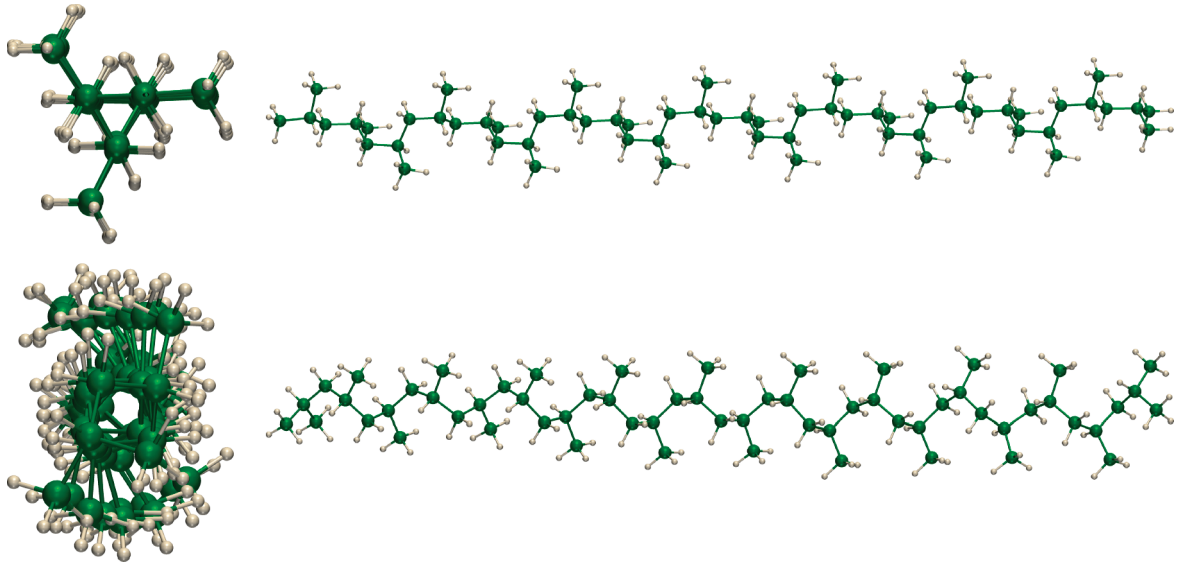

Figure 1. Sketch of the BP86/TZVP optimized geometry of $(TG)_{19}$ (top) and $(GG)_{19}$ (bottom) conformations of 20-unit isotactic polypropylene.

abilities needed in the VROA backward-scattering intensity expressions have been evaluated using the SNF program[45,53] by numerical differentiation. For this, the analytical energy gradients and the polarizability tensors were calculated with TURBOMOLE for distorted structures (of ±0.010 Bohr in the three directions of space for each atom away from the optimized geometry) using the same exchange-correlation functional and basis set as for the structure optimization. The BP86 vibrational frequencies were not multiplied by any scaling factor as they already agree with the experimental frequencies due to a systematic error cancellation.[54,55] For calculating the three polarizability tensors, a modified version[56] of TURBOMOLE's ESCF[57−60] program was used.

A typical incident light wavelength of 532 nm was adopted in all optical tensor calculations. This wavelength is clearly in the off-resonance regime. A Maxwell−Boltzmann T-dependence factor $(1/[1 - e^{(-\hbar\Delta\omega_p/(k_bT))}])$ has been added to eq 4 with $T = 298.15$ K to account for the T-dependence of the populations of the vibrational levels. In the spectra, each transition is represented by a Lorentzian function with full width at half-maximum (fwhm) of 10 cm^{-1}, which is more or less what is observed in the experimental spectra.[17]

The localization procedure and analysis in terms of GCMs, vibrational coupling matrices, and intensity coupling matrices has been performed using an add-on program to SNF written in Python.[37] Pictures of molecular structures and of the normal and localized modes of vibration have been prepared with the PyVib2 program.[61,62]

5. VROA Signatures of the Two Conformations

The two conformations $(TG)_{19}$ and $(GG)_{19}$ of the 20-unit isotactic polypropylene chain were optimized with BP86/TZVP. The resulting structures are shown in Figure 1. The $(TG)_{19}$ conformation turns out to have a very regular structure, and the $(GG)_{19}$ conformer is slightly distorted due to steric effects between the lateral methyl groups (see Supporting Information Table 1). For the $(TG)_{19}$ conformer, the root-mean-square deviations (rmsd) from the ideal 180° and 60° torsion angles are 1.0° and 0.6°, respectively, whereas for the $(GG)_{19}$ conformer the rmsd is 13.0°. The calculated Raman and VROA spectra are shown in Figure 2. Both spectra are quite different when going from the $(TG)_{19}$ to the $(GG)_{19}$ conformer. In the Raman spectra, the $(TG)_{19}$ spectrum is characterized by a succession of five peaks with similar magnitude while the $(GG)_{19}$ spectrum is dominated by three peaks. Moreover, the peak at 710 cm^{-1} is characteristic of the $(GG)_{19}$ conformation. The VROA spectra consist of a series of positive and negative peaks, which differ in magnitude and position in both conformations. In particular, the couplet (negative−positive) at around 1100 cm^{-1} in the VROA spectrum of the $(TG)_{19}$ conformation, highlighted in the blue rectangle, differs from the positive−negative−positive pattern observed in the spectrum of the $(GG)_{19}$ conformation. This difference might serve as a signature for distinguishing the $(TG)_{19}$ and $(GG)_{19}$ conformers, and our analysis will therefore focus on this specific feature of both spectra. Figure 3 displays the Raman and VROA spectra for the 20-unit chain and for a smaller 5-unit chain in order to observe the effect of the elongation of the chain. The Raman spectra are very alike, whereas in the VROA ones the patterns are conserved but the relative intensities of the peaks are changed. We observe, for instance, that the intensity of the positive peak (at 1075 cm^{-1}) in the couplet at around 1100 cm^{-1}, highlighted in the spectra, is decreased when elongating the chain. The spectra for the 5-unit chain are very similar to what has been published in ref 35 (top spectra in Figures 3 and 4 in ref 35) although the later have been calculated for 3-unit chains of polypropylene with Hartree−Fock and a smaller rDPS:3-21G basis set.[63] We may therefore directly compare our previous spectra of ref 35 with our new calculations here. We find that the signatures previously observed in ref 35 are still valid for longer chains and that the signatures are distinct between the spectra of the $(TG)_{19}$ and $(GG)_{19}$.

The different VROA signatures of 3-fold helical $(TG)_N$ and 4-fold $(GG)_N$ will now be investigated on 20-unit chains by using the localized mode procedure on a subset of bands, and we will pay particular attention to the couplet at around 1100 cm^{-1}. When looking closer at the frequencies and normal modes involved in this couplet, we observe two groups of modes separated by 45 cm^{-1} for the $(TG)_{19}$ conformation. Similarly, the corresponding modes for the $(GG)_{19}$ conformation are divided into two groups with a separation of 58 cm^{-1}. We have therefore two subsets of modes, two bands, that are analyzed

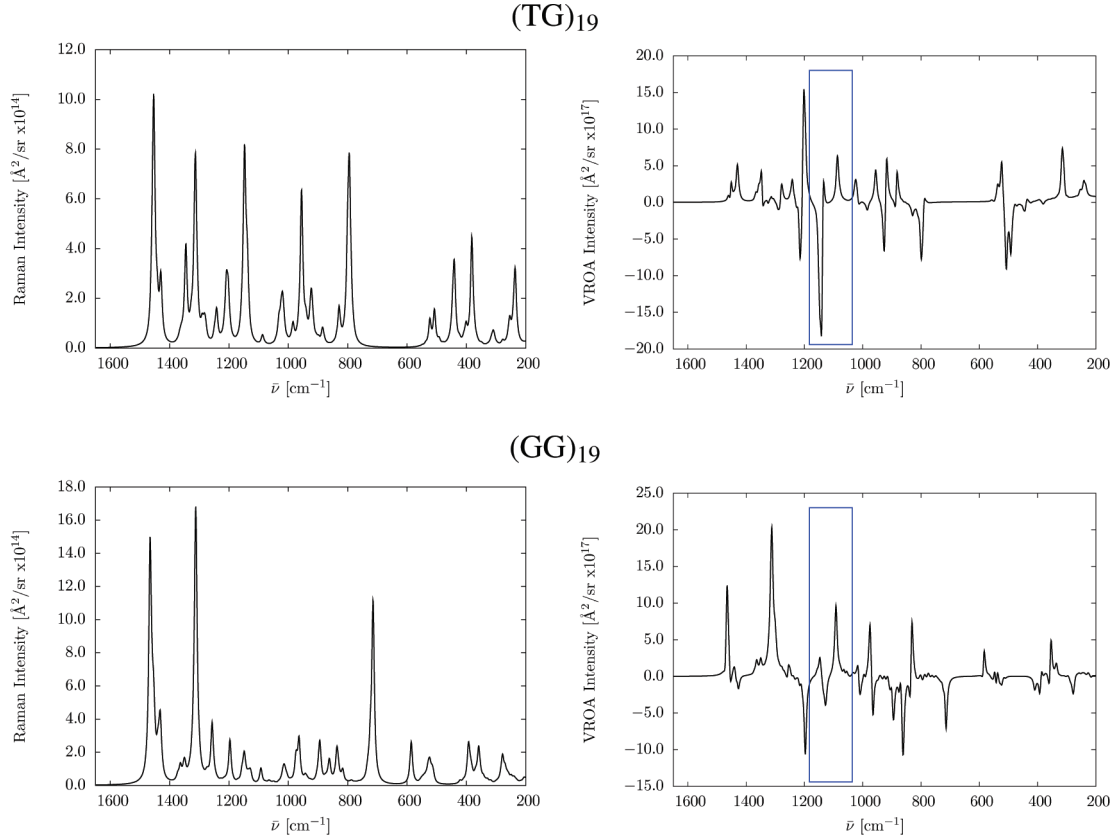

Figure 2. Calculated Raman polarized (left) and VROA backward-scattering (right) spectra of $(TG)_{19}$ (top) and $(GG)_{19}$ (bottom) conformations of 20-unit isotactic polypropylene.

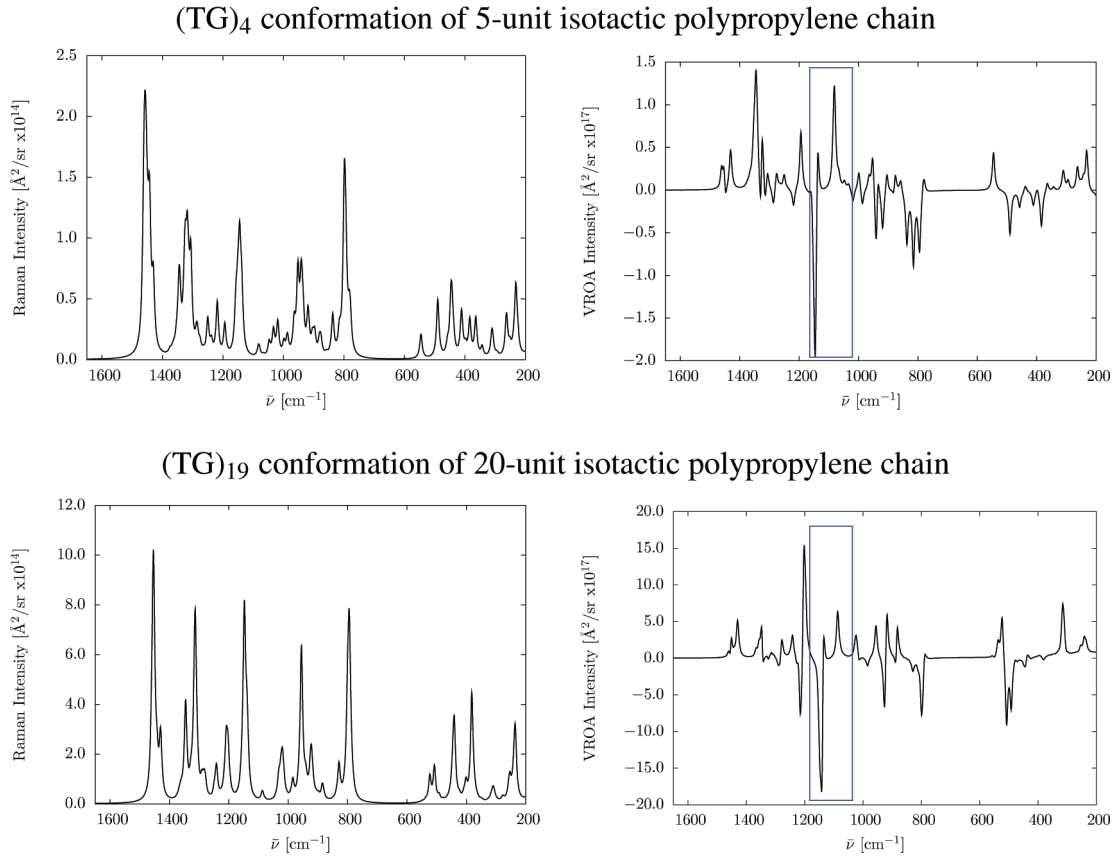

Figure 3. Calculated Raman polarized (left) and VROA backward-scattering (right) spectra of $(TG)_4$ conformation of 5-unit isotactic polypropylene chain (top) and of $(TG)_{19}$ conformation of 20-unit isotactic polypropylene chain (bottom).

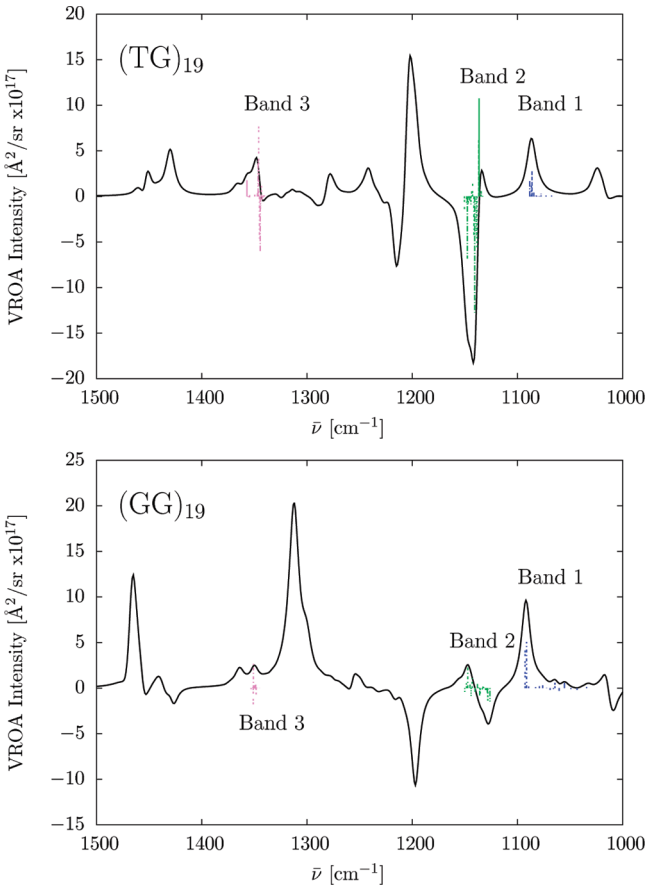

Figure 4. Calculated VROA backward-scattering spectra of $(TG)_{19}$ (top) and $(GG)_{19}$ (bottom) conformations of 20-unit isotactic polypropylene in the 1000 − 1500 cm^{-1} wavenumber range.

by the localization procedure. The low-frequency border of the first band and the high-frequency border of the second band are carefully chosen by inspecting the normal modes to only take those with similar displacement patterns. The fast convergence of the mode localization procedure is also an indication for the completeness of the subset of normal modes. A third band at higher frequency is analyzed in this work. Although it is not a signature of the helical conformation, this band was chosen because it displays a different displacement pattern in comparison to those of the first two bands (see Supporting Information Tables 2−7 for figures of all the normal modes under investigation). The atomic displacements for the modes in the first two bands involve mainly wagging motions of the hydrogens of the lateral methyl groups (two hydrogen atoms moves in the same direction while the third one is going in the opposite direction), and the atomic displacements for the modes in the third bands mainly involve wagging motions of the hydrogen atoms of the backbone (-C**H**$_2$- and -C**H**Me-). It is thus interesting to analyze the localized modes associated to this band as well as the vibrational and intensity coupling matrices in order to understand why they lead to quite small VROA intensities. Figure 4 shows more detailed VROA backward-scattering spectra for the $(TG)_{19}$ and $(GG)_{19}$ conformations in the 1000 − 1500 cm^{-1} region. The three bands under study are highlighted in blue, green and purple in the figure.

The mode localization procedure is then applied on each band. Figure 5 shows two normal modes and two localized modes belonging to the first band of the $(TG)_{19}$ conformation. The two normal modes involve similar wagging displacements of the atoms all over the chain. These specific displacements are highlighted in each of the localized modes that are very alike but located on two successive units. The localization procedure is therefore able to retrieve the displacement of the atoms of each unit independently.

6. Analysis of the Total Band Intensity

As mentioned before, the atomic displacements of the localized modes belonging to one band are similar and involve only a small set of atoms centered on one site of the chain (Figures 6 and 7, see Supporting Information Tables 8−13 for pictures of all the localized modes). The localized modes contains therefore the informations from one "unit cell" that is repeated along the axis of the chain. In the localization procedure, the phase between the localized modes is chosen such that they are as similar to each other as possible.

Within one band comprising a set of vibrational normal modes, the VROA backward-scattering intensities largely differs from each other to give a specific band shape. As an example, the first band of the $(TG)_{19}$ conformation has 13 contributing modes with VROA backward-scattering intensities ranging from -0.06×10^{-18} to 28.71×10^{-18} Å^2/sr. By contrast, the localized-mode intensities are far more similar (see Supporting Information Tables 14−19). The VROA backward-scattering intensities of to the localized modes range from 4.99×10^{-18} to 6.34×10^{-18} Å^2/sr. Of course, the sum of these intensities is equal to the total intensity of the band. We can thus analyze the total band intensity by observing the intensity of one representative localized mode only. This is done by using the GCM scheme of Hug in order to understand what atoms or groups of atoms are responsible for the localized-mode intensity (and thus for the total band intensity). As these localized modes involve only a few atoms, the GCM will be much smaller and thus easier to interpret compared to GCM patterns of normal modes.

6.1. $(TG)_{19}$ Conformation. The first investigated band appears in the 1070−1090 cm^{-1} frequency range. The localized modes, as shown in Figure 6 (see Supporting Information Table 8 for figures of all the localized modes), mainly involve H wagging motions of the lateral methyl groups as well as C−C stretching motions and span 4−5 units of the chain. The atomic displacement pattern is clearly similar to what was observed for the mode 35 of TGTG conformation of 3-unit polypropylene chain.[35] The localized mode frequencies (see Supporting Information Table 14) are very similar to each other with small discrepancies for the two modes which are at the termini of the chain. The VROA intensities are all positive and of similar amplitude, which leads to a positive total band intensity. We then analyze the GCM decomposition of the VROA intensity for one of the localized modes, which has its main contribution in the middle of the chain, between C^{19} and C^{28} of the backbone chain, (Figure 6). The largest contribution is the off-diagonal positive coupling term between C^{24} and C^{26}.

The second investigated band is situated just after the first, between 1130 cm^{-1} and 1150 cm^{-1}. Again, the vibrational frequencies of the localized modes are very similar to each other (see Supporting Information Table 15) with associated negative VROA intensities. The localized modes (see Supporting Information Table 9) are quite similar to those of the previous band except for a difference in phase factor inside the repetitive unit. Indeed, as can be seen from the sketch of the localized mode that has its main contribution between C^{19} and C^{28} (Figure 6), there is a phase difference for the displacement of the atoms C^{19}−C^{24} in comparison to the localized mode of the first band while the displacement of the C^{26}−C^{28} atoms has the same

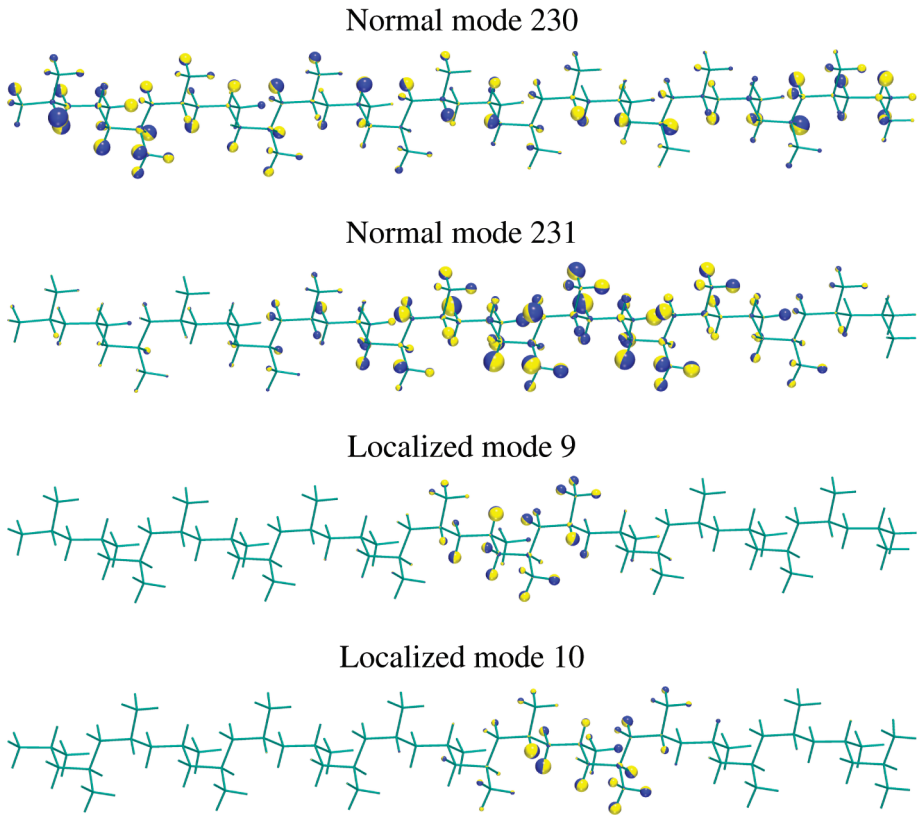

Figure 5. Sketch of two normal modes and two localized modes of the $(TG)_{19}$ conformation of the 20-unit isotactic polypropylene chain for Band 1 (mode 228 to mode 240).

phase. Moreover, the C^{25} H_2 motion is changed from a twisting to a rocking motion when going from band 1 to band 2. The GCM changes accordingly: the couplings between the groups with carbon atoms 19−24 and between the groups with carbon atoms 25−27 are mostly unchanged while the couplings between these two sets are reversed in sign when compared with the localized mode of band 1. The largest contribution is also given by the coupling between C^{24} and C^{26}.

The third investigated band, which is situated between 1340 and 1360 cm^{-1}, has a positive total band intensity that is smaller in magnitude than the two previous bands. The vibrational frequencies of the localized modes are similar to each other but their intensities are changing a bit more than for the two bands considered above (see Supporting Information Table 16). Nevertheless, the GCMs (see Supporting Information Table 22) look very similar to each other. The localized modes (Figure 6, see Supporting Information Table 10 for figures of all the localized modes) mainly consist of atomic displacements of the hydrogen atoms in C^{22}**H**Me, C^{23}**H**$_2$, and C^{24}**H**Me. Accordingly, the main GCM contributions are between C^{22}−C^{22}, C^{22}−C^{23}, C^{22}−C^{24}, C^{23}−C^{24}, and C^{24}−C^{24}. Among these, the two first and the two last couplings are negative and positive, respectively, and thus cancel each other. The sign can therefore be understood as the result of the coupling between the C^{22} HCH_3 and C^{24} HCH_3 groups.

6.2. $(GG)_{19}$ Conformation. For the $(GG)_{19}$ conformation, the corresponding three bands in the same zone of frequencies are analyzed. The first band is situated between 1030 and 1095 cm^{-1}. As for the $(TG)_{19}$ conformation, the total band intensity is positive. Again, this is reflected by the intensities of the localized modes (see Supporting Information Table 17). For the second band situated between 1120 and 1150 cm^{-1}, the total intensity is small in magnitude and negative (see Supporting Information Table 18). This is similar to what was found for the $(TG)_{19}$ conformation, where the total intensity is also negative, but somewhat larger in magnitude. The same kinds of H wagging and C−C stretching motions are found for the localized modes of the first two bands of the $(GG)_{19}$ conformer (Figure 7, see Supporting Information Table 11 and 12 for figures of all the localized modes) as for the $(TG)_{19}$ conformer. Even though the geometries and helical pitches of the two conformers are quite different, we can still compare the localized modes obtained from both bands (Figure 7). A similar vibration as observed for the $(TG)_{19}$ conformer is found here: the displacements of the C^{19}−C^{25} moiety are similar for both bands while the displacements of the C^{26}−C^{28} moiety have opposite phase. This has a direct impact on the group-coupling matrices. Indeed, for the first band, the C^{20}−C^{26} group coupling is positive and it is negative for the C^{24}−C^{26}, whereas both couplings are characterized by negative intensities for the localized mode of the second band. This leads to the total intensities of band 1 and band 2 having opposite signs. In summary, for both conformers, band 1 and 2 are generated by similar vibrations, which—due to a phase difference between the localized modes—have opposite total intensities. The differences between the two conformers are, therefore, due to the band shapes, which will be analyzed in the following section.

The third band, between 1345 and 1355 cm^{-1}, has a relatively small VROA backward-scattering intensity (see Supporting Information Table 19). The localized modes (Figure 7, see Supporting Information Table 13 for figures of all the localized modes) consist of H wagging motions of the hydrogen atoms on the backbone, as seen for the $(TG)_{19}$ conformer, as well as an umbrella mode of the lateral methyl groups. The GCM of the reference local mode (Figure 7) is composed of negative and positive contributions that are canceling each other.

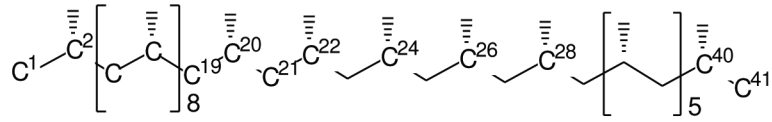

Band 1

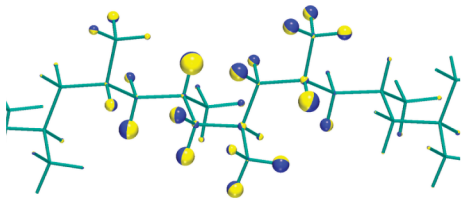

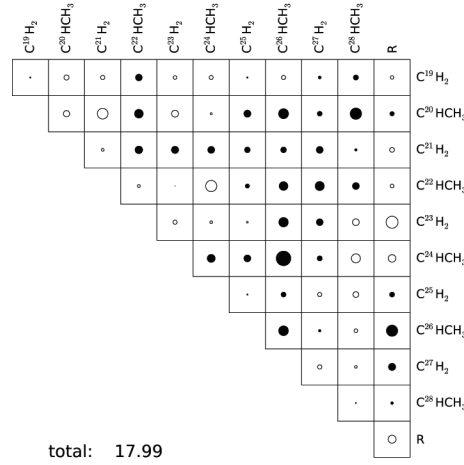

Band 2

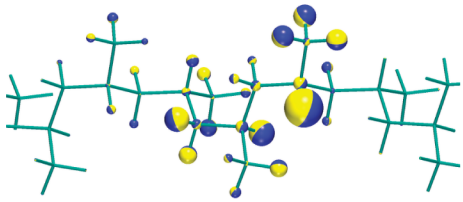

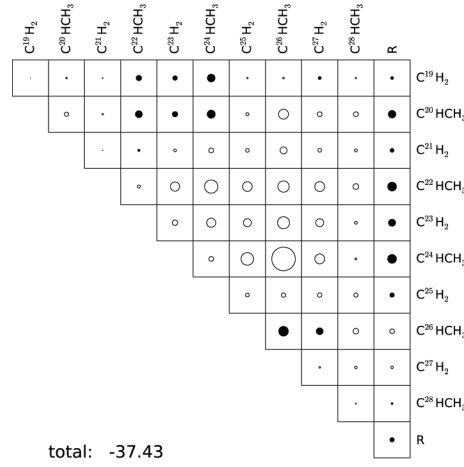

Band 3

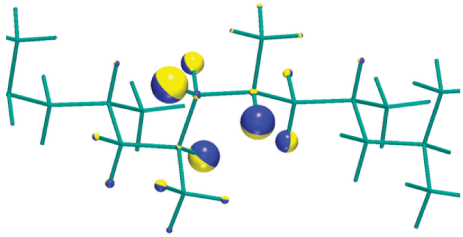

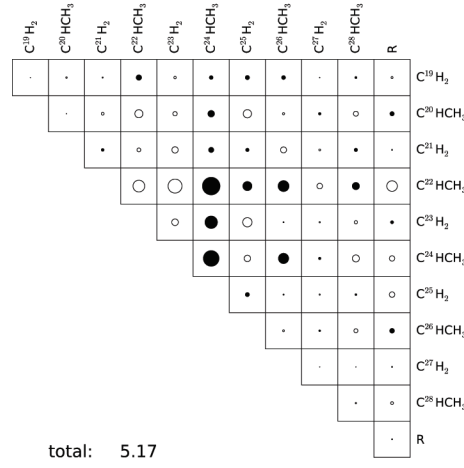

Figure 6. Sketch of a representative localized mode (left) and the corresponding VROA backward-scattering group coupling matrix analysis (right) for the three considered bands of the $(TG)_{19}$ conformation of 20-unit isotactic polypropylene. The direction of atomic displacements is perpendicular to the junction plane between the two hemispheres of distinct color while their amplitudes are proportional to the radius of the sphere. For the GCMs, the groups are formed by one carbon atom from the backbone together with its side atoms (see the Lewis structure for the numbering of the atoms). The black (white) circles indicate positive (negative) contributions to the VROA backward-scattering intensity while the area of the circles are proportional to their amplitudes. The total VROA backward-scattering intensities of the localized modes (in Å^4/amu) are also given.

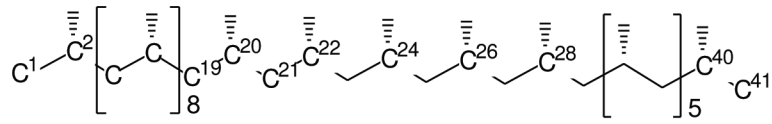

Band 1

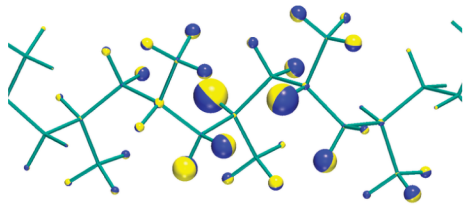

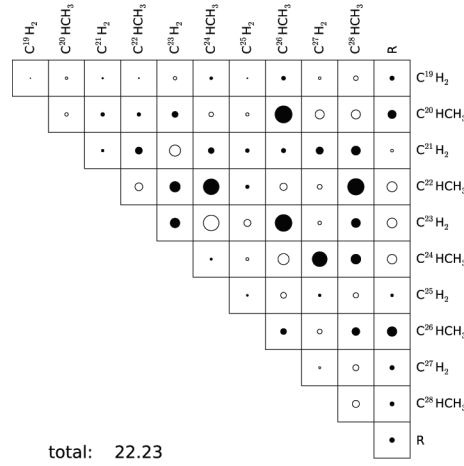

Band 2

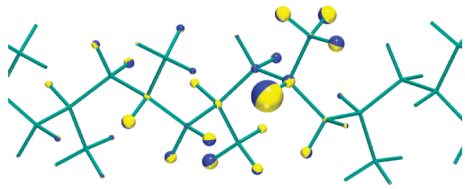

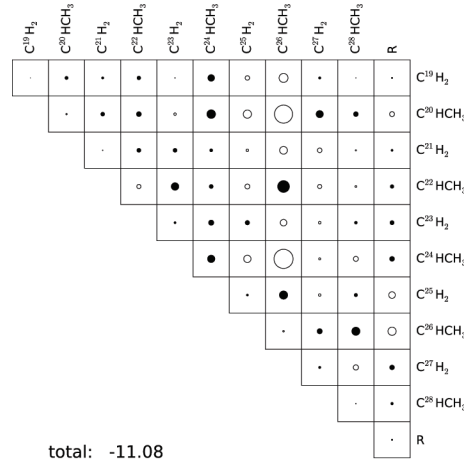

Band 3

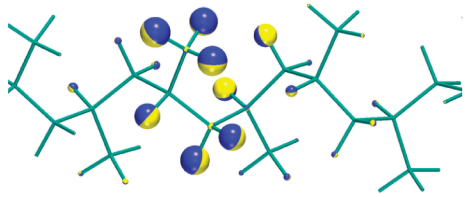

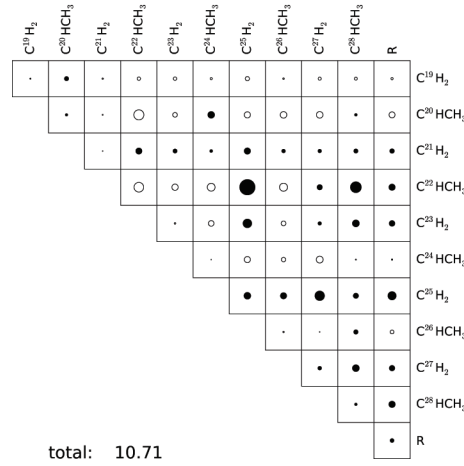

Figure 7. Sketch of a representative localized mode (left) and the corresponding VROA backward-scattering group coupling matrix analysis (right) for the three considered bands of the $(GG)_{19}$ conformation of 20-unit isotactic polypropylene. The direction of atomic displacements is perpendicular to the junction plane between the two hemispheres of distinct color while their amplitudes are proportional to the radius of the sphere. For the GCMs, the groups are formed by one carbon atom from the backbone together with its side atoms (see the Lewis structure for the numbering of the atoms). The black (white) circles indicate positive (negative) contributions to the VROA backward-scattering intensity while the area of the circles are proportional to their amplitudes. The total VROA backward-scattering intensities of the localized modes (in $Å^4$/amu) are also given.

TABLE 1: Subblock of the Localized Modes Coupling Matrix $\tilde{\Omega}$ for the Normal Modes of 20-Unit $(TG)_{19}$ Isotactic Polypropylene

Band 1 (mode 228 to mode 240)

1082.7	−0.4	3.4	1.4	−0.7	−0.4	0.3	0.2
−0.4	1082.2	1.2	3.3	−1.7	−1.0	0.5	0.3
3.4	1.2	1082.7	−0.3	3.4	1.3	−0.8	−0.4
1.4	3.3	−0.3	1082.0	1.1	3.2	−1.7	−0.8
−0.7	−1.7	3.4	1.1	1082.4	−0.3	3.6	1.3
−0.4	−1.0	1.3	3.2	−0.3	1081.8	1.1	3.0
0.3	0.5	−0.8	−1.7	3.6	1.1	1082.3	−0.3
0.2	0.3	−0.4	−0.8	1.3	3.0	−0.3	1081.8

Band 2 (mode 241 to mode 259)

1141.1	−0.0	3.8	0.0	−0.2	−0.1	0.1	−0.0
−0.0	1140.5	0.1	3.7	0.3	−0.3	−0.1	0.1
3.8	0.1	1140.6	−0.2	3.6	0.4	−0.3	−0.2
0.0	3.7	−0.2	1140.9	−0.1	3.7	0.1	−0.2
−0.2	0.3	3.6	−0.1	1140.4	−0.1	3.6	0.3
−0.1	−0.3	0.4	3.7	−0.1	1140.4	−0.2	3.6
0.1	−0.1	−0.3	0.1	3.6	−0.2	1140.9	−0.1
−0.0	0.1	−0.2	−0.2	0.3	3.6	−0.1	1140.5

Band 3 (mode 322 to mode 342)

1347.0	1.4	2.4	1.5	0.3	−0.0	−0.0	0.0
1.4	1346.8	0.8	2.5	1.5	0.3	0.0	−0.0
2.4	0.8	1346.5	1.2	2.5	1.3	0.3	−0.0
1.5	2.5	1.2	1346.9	1.4	2.4	1.5	0.3
0.3	1.5	2.5	1.4	1346.6	0.9	2.4	1.4
−0.0	0.3	1.3	2.4	0.9	1346.5	1.2	2.5
−0.0	0.0	0.3	1.5	2.4	1.2	1346.9	1.4
0.0	−0.0	−0.0	0.3	1.4	2.5	1.4	1346.5

7. Analysis of the Band Shapes

To analyze the band shapes, one needs to understand how the localized modes couple to form the normal modes and how the VROA intensity is distributed among the normal modes. The coupling between the localized modes is given by the vibrational coupling matrix $\tilde{\Omega}$, where the diagonal elements represent the vibrational frequencies of the localized modes and where the off-diagonal terms are the vibrational coupling constants. These coupling terms determine the mixing between the localized modes in the vibrational normal modes. If only the nearest-neighbor coupling constants are large, then the coupling pattern is very simple: the vibrational normal modes consist in the linear evolution from the nodeless in-phase combination of the localized modes to an out-of-phase combination with a maximum number of nodes. If the coupling terms are positive, the in-phase (nodeless) combination is found at higher wavenumbers and the out-of-phase combination at lower wavenumbers. For negative coupling terms, the opposite order is obtained. If the second-nearest neighbor coupling constants are the dominant coupling terms, then the localized modes have a degeneracy of two. For example, if we consider the mixing of six localized modes, the result will be two nodeless normal modes, two normal modes with one node, and two normal modes with two nodes. The ordering for positive coupling terms is again the in-phase combination at higher wavenumbers and the out-of-phase combination at lower wavenumbers.

In the following subsections, we analyze the band shapes by investigating which combinations of localized modes arise from the vibrational coupling constant patterns and how the VROA intensity is distributed among these modes due to the intensity coupling terms. Nevertheless, the number of localized modes makes the analysis still difficult to conduct. We therefore analyze only a small block of the vibrational coupling and intensity coupling matrices. This block is chosen such that the localized modes involved correspond to displacements of the middle of the chain. The diagonalization of such a sub-block of the vibrational coupling matrix therefore gives a set of "optimum" normal modes in a sense that only the most regular part of the chain is kept.

7.1. $(TG)_{19}$ Conformation. The first band consists of positive peaks with the most intense ones at higher wavenumber (see Supporting Information Table 14). For the second band, the lowest wavenumber bands are positive while the bands in the middle and higher wavenumbers are negative (see Supporting Information Table 15). These differences can be understood by the vibrational coupling matrices (Table 1) and by the intensity coupling matrices (Figure 8).

The vibrational coupling matrix for the first peak is more complex than the two simple cases discussed before. Indeed, the second-neighbor coupling constants are the largest, but the third-neighbor couplings are also important and are usually larger than the first-neighbor terms. This results in a quite

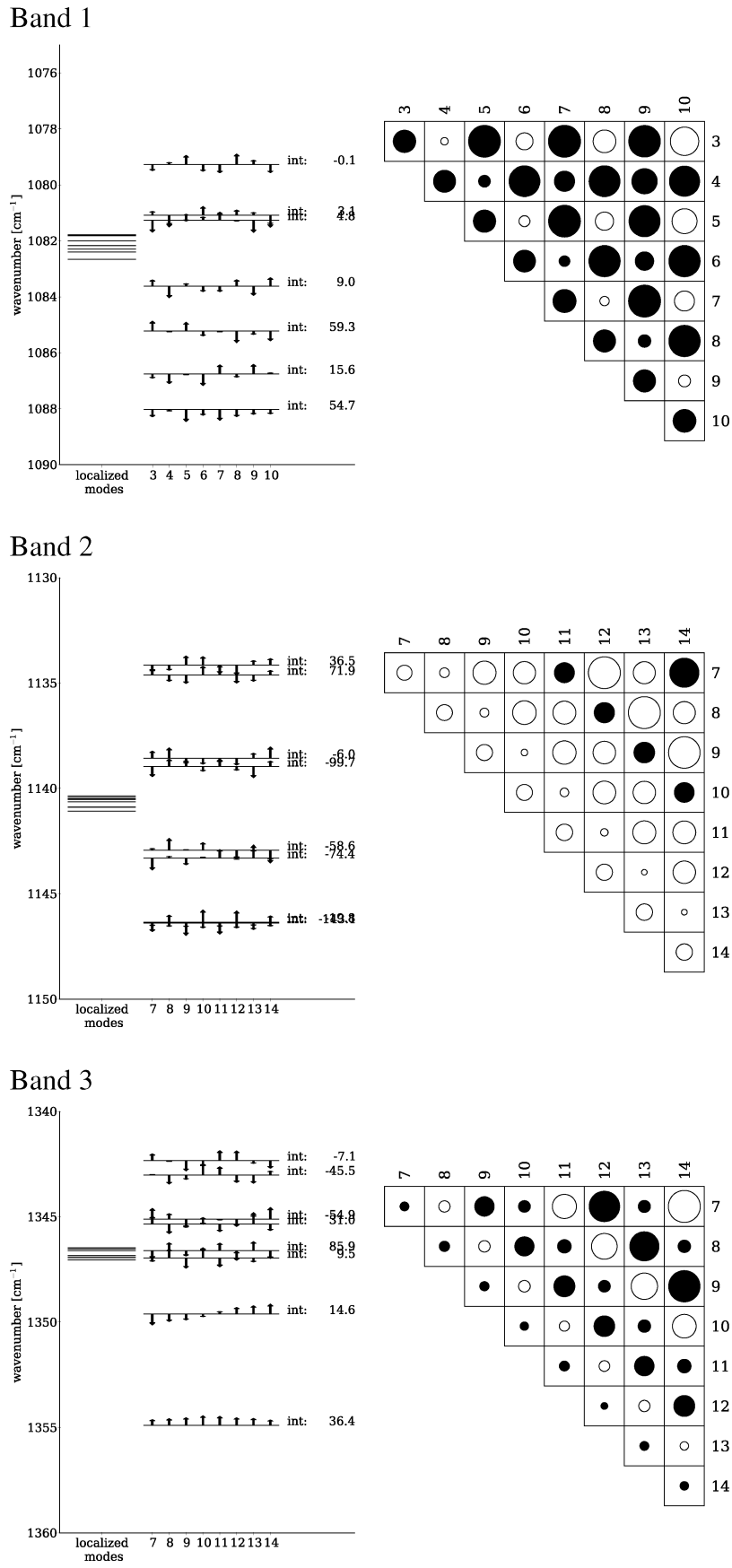

Figure 8. Representation of the transformation matrices **U** (left) and subblock of the intensity coupling matrices (right) of representative localized modes of the $(TG)_{19}$ conformation of 20-unit isotactic polypropylene. The arrows on one line indicate the contributions of the subblock of localized modes (given by U_{pq}) to the normal mode p. The areas of circles are directly proportional to the intensity coupling terms ($\tilde{I}_{qr}$) with black (white) colors indicating positive (negative) contributions.

TABLE 2: Subblock of the Localized Modes Coupling Matrix $\tilde{\Omega}$ for the Normal Modes of 20-Unit $(GG)_{19}$ Isotactic Polypropylene

Band 1 (mode 226 to mode 240)

$$\begin{pmatrix} 1066.5 & -12.0 & -4.8 & -3.4 & -0.7 & -0.8 & -0.4 & -0.3 \\ -12.0 & 1066.9 & -12.0 & -1.5 & -1.2 & -0.0 & -0.1 & -0.0 \\ -4.8 & -12.0 & 1064.4 & -13.3 & -1.8 & -2.8 & -0.6 & -0.3 \\ -3.4 & -1.5 & -13.3 & 1065.7 & -14.6 & -0.8 & -2.4 & -0.1 \\ -0.7 & -1.2 & -1.8 & -14.6 & 1070.0 & -12.5 & -3.6 & -2.0 \\ -0.8 & -0.0 & -2.8 & -0.8 & -12.5 & 1069.5 & -9.5 & -1.5 \\ -0.4 & -0.1 & -0.6 & -2.4 & -3.6 & -9.5 & 1067.1 & -11.5 \\ -0.3 & -0.0 & -0.3 & -0.1 & -2.0 & -1.5 & -11.5 & 1073.2 \end{pmatrix}$$

Band 2 (mode 242 to mode 260)

$$\begin{pmatrix} 1137.2 & 3.6 & 2.6 & 1.1 & -1.0 & 0.3 & -0.0 & -0.0 \\ 3.6 & 1137.4 & 2.6 & 3.6 & 0.7 & -0.8 & 0.1 & 0.0 \\ 2.6 & 2.6 & 1135.3 & 3.0 & 2.6 & 1.8 & -0.9 & 0.2 \\ 1.1 & 3.6 & 3.0 & 1134.3 & 3.9 & 1.5 & 2.0 & -1.1 \\ -1.0 & 0.7 & 2.6 & 3.9 & 1135.8 & 3.3 & 2.2 & 1.3 \\ 0.3 & -0.8 & 1.8 & 1.5 & 3.3 & 1139.2 & 2.2 & 3.5 \\ -0.0 & 0.1 & -0.9 & 2.0 & 2.2 & 2.2 & 1136.0 & 3.4 \\ -0.0 & 0.0 & 0.2 & -1.1 & 1.3 & 3.5 & 3.4 & 1134.7 \end{pmatrix}$$

Band 3 (mode 322 to mode 341)

$$\begin{pmatrix} 1349.9 & -0.3 & 0.1 & 0.4 & 0.1 & 0.0 & 0.1 & -0.0 & 0.0 & 0.0 \\ -0.3 & 1349.5 & -0.0 & -0.2 & 0.3 & -0.0 & 0.1 & -0.0 & -0.0 & -0.0 \\ 0.1 & -0.0 & 1350.0 & 0.1 & 0.1 & 0.5 & -0.1 & 0.1 & -0.0 & -0.0 \\ 0.4 & -0.2 & 0.1 & 1348.4 & 0.2 & 0.3 & 0.4 & 0.2 & 0.0 & 0.0 \\ 0.1 & 0.3 & 0.1 & 0.2 & 1349.0 & 0.2 & 0.1 & 0.4 & 0.1 & 0.1 \\ 0.0 & -0.0 & 0.5 & 0.3 & 0.2 & 1349.9 & 0.4 & -0.3 & 0.5 & -0.0 \\ 0.1 & 0.1 & -0.1 & 0.4 & 0.1 & 0.4 & 1349.6 & -0.4 & 0.2 & 0.5 \\ -0.0 & -0.0 & 0.1 & 0.2 & 0.4 & -0.3 & -0.4 & 1348.2 & -0.0 & 0.1 \\ 0.0 & -0.0 & -0.0 & 0.0 & 0.1 & 0.5 & 0.2 & -0.0 & 1349.7 & 0.5 \\ 0.0 & -0.0 & -0.0 & 0.0 & 0.1 & -0.0 & 0.5 & 0.1 & 0.5 & 1349.8 \end{pmatrix}$$

complicated pattern, where all the normal modes have two or more nodes, but nevertheless, the modes at higher wavenumbers have less nodes (Figure 8). The intensity coupling matrix is simpler with the diagonal and second, fourth, and sixth off-diagonal lines containing only positive terms. On the other hand, the odd off-diagonal lines contain smaller terms with alternating signs. As a consequence of this pattern dominated by positive terms, the modes at higher wavenumber that have fewer nodes give rise to intense and positive peaks while the modes with more nodes will give less-intense peaks due to cancellation of the positive terms.

For the second band, the vibrational coupling matrix is dominated by the positive second-neighbor coupling terms. The resulting pattern of the coupling is quite simple and consists, as explained before, of nearly degenerated peaks of similar number of nodes (Figure 8). Since the couplings are positive, the combination with few nodes are situated at higher wavenumbers. The intensity coupling matrix is dominated by negative contributions while the fourth off-diagonal line contains positive terms. Therefore, the peaks with few nodes will be associated with negative intensities whereas for the peaks with many nodes the intensities cancel or even reverse into positive contributions. Overall, the mainly negative intensity for band 2 and the positive intensity at band 1 together lead to the couplet identified as a signature of the $(TG)_N$ conformation.

The vibrational coupling matrix of the third peak consists of positive terms for both nearest-, second-, and third-nearest neighbors. The pattern for the normal modes is therefore difficult to predict. Nevertheless, we can observe that the nodeless and one-node modes are at higher wavenumbers while the normal modes with the highest number of modes are in the middle. The peaks at higher wavenumbers have positive intensities since the intensity coupling matrix is dominated by positive combinations (second, third, and fifth off-diagonal lines). When the number of nodes increases, the intensities become more difficult to predict but are, however, mainly negative.

7.2. $(GG)_{19}$ Conformation. For the $(GG)_N$ conformation, the first band is mostly made up from modes with positive intensity at the higher wavenumber end, while for the second band, there are modes with positive intensity at higher wavenumbers and modes with negative intensity at lower wavenumbers (see Supporting Information Tables 17 and 18). For the first band, the vibrational coupling matrix (Table 2) is dominated by the negative nearest-neighbor contributions. Therefore, the modes display a simple pattern: a linear evolution of the number of nodes from the in-phase combination at low frequency to maximum number of nodes at high frequency (Figure 9). The intensity coupling matrix consists of an alternation of positive and negative contributions. For the nodeless combination of localized modes, the intensity coupling terms cancel each other and give rise to a slightly positive peak. For the next modes, with few numbers of nodes, the intensities are small in magnitude, whereas with increasing numbers of nodes, some negative contributions reverse sign, leading to intense positive peaks. Note that, even though the same final band shape arises, this is different from the $(TG)_N$ conformation. Both the order

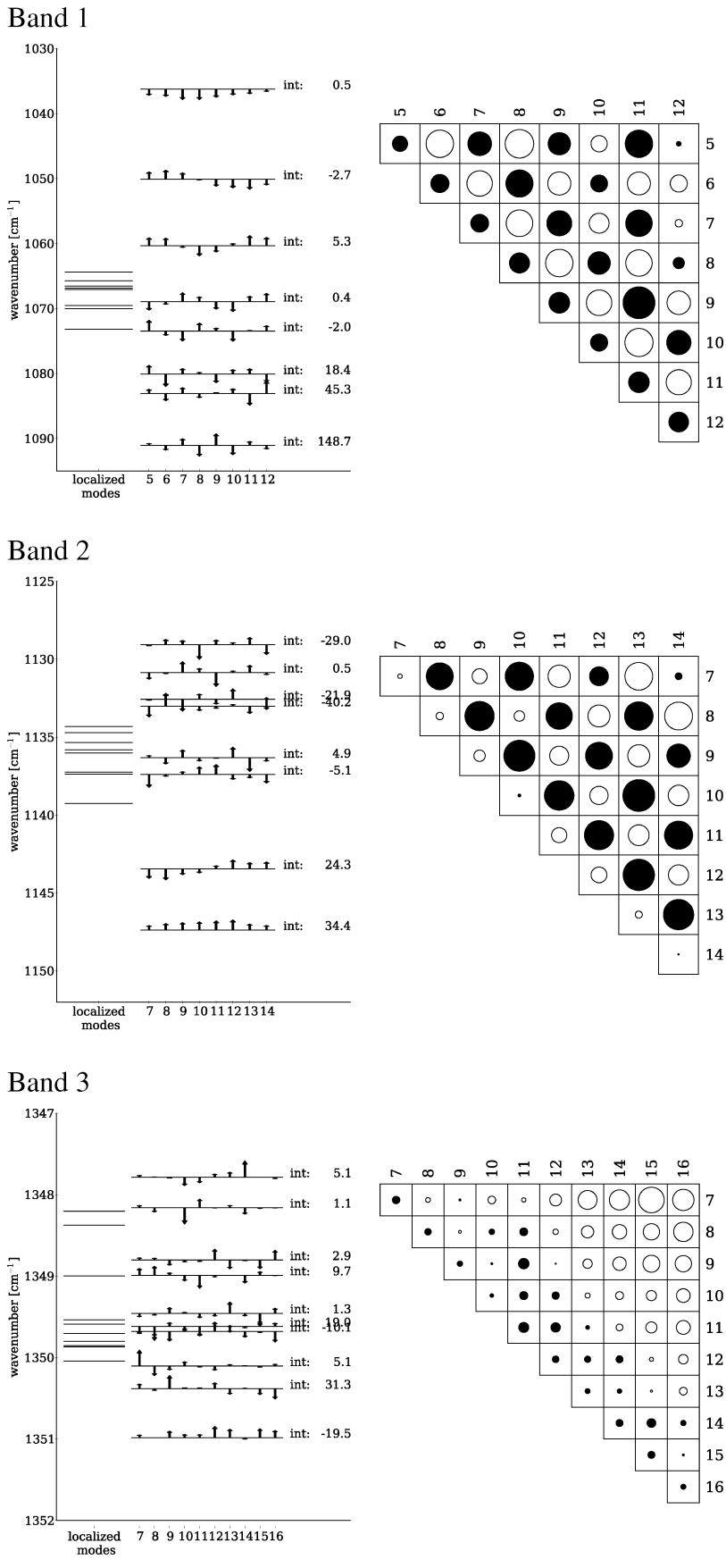

Figure 9. Representation of the transformation matrices **U** (left) and subblock of the intensity coupling matrices (right) of representative localized modes of the $(GG)_{19}$ conformation of 20-unit isotactic polypropylene. The arrows on one line indicate the contributions of the subblock of localized modes (given by U_{pq}) to the normal mode p. The areas of circles are directly proportional to the intensity coupling terms ($\tilde{I}_{qr}$) with black (white) colors indicating positive (negative) contributions.

TABLE 3: Summary of the Observations for the Band Shape Based on the Analysis of the Vibrational and Intensity Coupling Matrices

	band 1	band 2	band 3
		$(TG)_{19}$ Conformation	
$\tilde{\mathbf{\Omega}}$	positive second-neighbor terms + other smaller contributions	positive second-neighbor terms	positive nearest, second, and third-neighbor terms
$\tilde{\mathbf{I}}$	positive terms	negative terms	alternating positive and negative terms
band shape	high wavenumber modes have few nodes and intense positive intensities.	high wavenumber modes have few nodes and intense negative intensities.	high wavenumber modes have few nodes and positive intensities.
		$(GG)_{19}$ Conformation	
$\tilde{\mathbf{\Omega}}$	negative nearest-neighbor terms	positive nearest, second, and third-neighbor terms	small coupling terms
$\tilde{\mathbf{I}}$	alternating positive and negative terms	alternating negative and positive terms	positive terms for the short-range couplings and negative terms for long-range couplings
band shape	high wavenumber modes have many nodes and intense positive intensities.	high wavenumber modes have few nodes and positive intensities. modes with many nodes have negative intensities.	one-node and nodeless modes at high wavenumber give intense positive and negative peaks, respectively.

of the coupled normal modes and the distribution of intensity among them are inverted with respect to the $(TG)_N$ conformation.

In the second band, both the order of the peaks and the intensity coupling pattern are reversed compared to the first band. The nearest-, second-, and third-neighbor coupling terms of $\tilde{\mathbf{\Omega}}$ are all important and positive (Table 2). This pattern was already observed for the third band of the $(TG)_{19}$ conformation. The in-phase combination is therefore at higher wavenumber while the modes with a large number of nodes are situated in the middle of the frequency range. The intensity coupling matrix is similar but opposite to the coupling matrix of the first band (Figure 9). Thus, the in-phase combination leads to a positive peak (again due to the cancellation of the intensity terms) at high wavenumber. The peaks with the larger magnitude but negative intensities originate from the modes with the highest number of nodes (in contrast to the intense positive peak at high frequency as seen for the first band) in the middle of the frequency range. Therefore, in contrast to the mainly negative second band found for the $(TG)_{19}$ conformation, for the $(GG)_{19}$ conformation the second band is split into a positive-negative couplet. Together with the positive first band, this leads to the characteristic positive-negative-positive pattern.

The third band presents very weak coupling terms (Table 2). The coupling pattern is therefore very difficult to predict even if a nodeless and a one-node combination can be recognized at high frequency. The intensity coupling matrix is also quite peculiar (Figure 9) with positive diagonal, first, and second off-diagonal terms and all the other off-diagonal elements being negative. Since the number of nodes is quite high, these contributions mainly cancel each other and thus give rise to small positive and negative peaks. Only the two last modes at high frequency, namely, the one-node and the nodeless combination, give rather intense positive and negative peaks, respectively.

8. Conclusions

The previous investigation of VROA signatures on a small oligomer of polypropylene[35] showed that VROA spectroscopy exhibits special fingerprints for the different conformations of the chain. A couplet at around 1100 cm^{-1} was assigned to the 3-fold helicity (TGTG conformation). Nevertheless, without appropriate tools, it was difficult to analyze longer polymer chains since the number of modes, and therefore the quantity of information to analyze, increases with the size of the system. With a new tool to analyze the modes of vibration and the VROA intensities developed,[37] we have investigated the difference of signatures between the 3-fold $(TG)_N$ and 4-fold $(GG)_N$ conformations for an isotactic polypropylene chain of relatively long size (20 units). We have particularly focused on the couplet at around 1100 cm^{-1} that was described as a signature of the $(TG)_N$ conformation of the 3-unit chain[35] and on the corresponding signature for the $(GG)_N$ conformation. Indeed, their Raman and VROA spectra show distinct signatures. From the comparison of spectra for a smaller 5-unit chain we have concluded that the signatures observed for the 3-unit chain[35] are conserved when elongating the chain.

Three bands in the VROA spectra of $(TG)_{19}$ and $(GG)_{19}$ conformations have been analyzed with the mode localization procedure. The two first bands correspond to the couplet at 1100 cm^{-1} for the $(TG)_{19}$ conformation. The GCMs for the $(TG)_{19}$ conformation show that the couplet arises from a difference of phase within the localized modes of both peaks, leading to the inversion of the sign of the total VROA intensity between the two bands. A similar observation is found for the VROA intensity of the two first bands of the $(GG)_{19}$ conformation. Therefore, the difference between the spectra are explained by the difference in their band shape. Table 3 presents a summary of the analysis on the vibrational and intensity coupling matrices. The first bands of both conformations have a similar band shapes but for different reasons since both the vibrational and the intensity coupling matrices are different. For the second peak, it is mainly the intensity coupling matrices that differ and give rise to two different band shapes. Both the vibrational and the intensity coupling terms mainly depend on the orientation of the localized modes with respect to each other. Therefore, we can be confident that the identified signatures are directly connected to the different helical pitch of the two conformers.

The third band under study is characterized by very different atomic contributions of the localized modes. These modes involve wagging motions of the hydrogen atoms of the backbone. The GCMs for both $(TG)_{19}$ and $(GG)_{19}$ conformers contain positive and negative terms that nearly cancel each other resulting in relatively small VROA intensities.

In conclusion, the mode localization analysis clearly shows that the difference in the VROA-intensity signatures between the $(TG)_N$ and $(GG)_N$ conformers can be rationalized in terms

of different localized modes and their corresponding vibrational coupling and intensity coupling matrices. Such analysis can be generalized to other synthetic or biological polymers and again demonstrates the great sensitivity of VROA upon conformational changes. In addition, one needs to have tools such as the mode localization approach to analyze these effects on the vibrational spectra.

Acknowledgment. V.L. thanks the FRS-FNRS for his Postdoctoral Researcher position. M.R. thanks the Swiss National Science Foundation (SNF) for financial support (project 200020-121870). C.R.J. acknowledges funding through a Rubicon scholarship of The Netherlands Organization for Scientific Research (NWO).

Supporting Information Available: The Supporting Information contains sketches of all the normal modes and localized modes under investigation as well as graphic representations of the group coupling matrices and the intensity coupling matrices $\tilde{\mathbf{I}}$. Tables with the VROA backward-scattering intensities associated to the normal modes and the localized modes and Tables with the values for the vibrational coupling matrices $\tilde{\mathbf{\Omega}}$ are also included there. The torsion angles of the backbone of the $(TG)_{19}$ and $(GG)_{19}$ conformers of the 20-unit isotactic polypropylene chain after optimization with the BP86 exchange-correlation functional and the TZVP basis set are given as well in Table 1 of the Supporting Information. This information is available free of charge via the Internet at http://pubs.acs.org.

References and Notes

(1) Bower, D. I.; Maddams, W. F. *The Vibrational Spectroscopy of Polymers*; Cambridge University Press: Cambridge, 1992.
(2) Zerbi, G. *Modern Polymer Spectroscopy*; Wiley-VCH: Weinheim, 1999.
(3) Zerbi, G.; Del Zoppo, M. *J. Chem. Soc. Faraday Trans.* **1992**, *88*, 1835.
(4) Orendorff, C. J.; Ducey, M. W. J.; Pemberton, J. E. *J. Phys. Chem. A* **2002**, *106*, 6991.
(5) Demoustier-Champagne, S.; Stavaux, P. Y. *Chem. Mater.* **1999**, *11*, 829.
(6) Clavell-Grunbaum, D.; Strauss, H. L.; Snyder, R. G. *J. Phys. Chem. B* **1997**, *101*, 335.
(7) Barron, L. D.; Buckingham, A. D. *Mol. Phys.* **1971**, *20*, 1111.
(8) Hug, W. In *Handbook of Vibrational Spectroscopy*; Chalmers, J. M., Griffiths, P. R., Eds.; John Wiley and Sons: Chichester, 2002; Vol. 1, p175.
(9) Barron, L. D. *Molecular Light Scattering and Optical Activity*; Cambridge University Press: Cambridge, 2004.
(10) Barron, L. D.; Hecht, L.; Gargaro, A. R.; Hug, W. *J. Raman Spectrosc.* **1990**, *21*, 375–379.
(11) Costante, J.; Hecht, L.; Polavarapu, P. L.; Collet, A.; Barron, L. D. *Angew. Chem., Int. Ed.* **1997**, *36*, 885–887.
(12) Hug, W.; Zuber, G.; de Meijere, A.; Khlebnikov, A.; Hansen, H.-J. *Helv. Chim. Acta* **2001**, *84*, 1–21.
(13) Ruud, K.; Helgaker, T.; Bour, P. *J. Phys. Chem. A* **2002**, *106*, 7448–7455.
(14) Bour, P.; Sychrovsky, V.; Malon, P.; Hanzlikova, J.; Baumruk, V.; Pospisek, J.; Budesinsky, M. *J. Phys. Chem. A* **2002**, *106*, 7321–7327.
(15) Pecul, M.; Rizzo, A.; Leszczynski, J. *J. Phys. Chem. A* **2002**, *106*, 11008–11016.
(16) Barron, L. D.; Hecht, L.; McColl, I. H.; Blanch, E. W. *Mol. Phys.* **2004**, *102*, 731–744.
(17) Zuber, G.; Hug, W. *Helv. Chim. Acta* **2004**, *87*, 2208–2234.
(18) Reiher, M.; Liégeois, V.; Ruud, K. *J. Phys. Chem. A* **2005**, *109*, 7567–7574.
(19) Zuber, G.; Goldsmith, M.-R.; Beratan, D. N.; Wipf, P. *ChemPhysChem* **2005**, *6*, 595–597.
(20) Haesler, J.; Schindelholz, I.; Riguet, E.; Bochet, C. G.; Hug, W. *Nature* **2007**, *446*, 526–529.
(21) Hug, W.; Haesler, J.; Kozhushkov, S. I.; de Meijere, A. *ChemPhysChem* **2007**, *8*, 1161–1169.
(22) Haesler, J.; Hug, W. *Chimia* **2008**, *62*, 482–488.
(23) Blanch, E. W.; Hecht, L.; Barron, L. D. *Methods* **2003**, *29*, 196–209.
(24) Budesinsky, M.; Sebestik, J.; Bednarova, L.; Baumruk, V.; Safarik, M.; Bour, P. *J. Org. Chem.* **2008**, *73*, 1481–1489.
(25) Hobro, A. J.; Rouhi, M.; Conn, G. L.; Blanch, E. W. *Vib. Spectrosc.* **2008**, *48*, 37–43.
(26) Jacob, Ch. R.; Luber, S.; Reiher, M. *ChemPhysChem* **2008**, *9*, 2177–2180.
(27) Herrmann, C.; Ruud, K.; Reiher, M. *Chem. Phys.* **2008**, *343*, 200–209.
(28) Kapitan, J.; Zhu, F.; Hecht, L.; Gardiner, J.; Seebach, D.; Barron, L. D. *Angew. Chem., Int. Ed.* **2008**, *47*, 6392–6394.
(29) Deplazes, E.; van Bronswijk, W.; Zhu, F.; Barron, L. D.; Ma, S.; Nafie, L. A.; Jalkanen, K. J. *Theor. Chem. Acc.* **2008**, *119*, 155–176.
(30) Mukhopadhyay, P.; Zuber, G.; Beratan, D. N. *Biophys. J.* **2008**, *95*, 5574–5586.
(31) Ashton, L.; Blanch, E. W. *Appl. Spectrosc.* **2008**, *62*, 469–475.
(32) Liégeois, V.; Quinet, O.; Champagne, B. *J. Chem. Phys.* **2005**, *122*, 214304.
(33) Liégeois, V.; Quinet, O.; Champagne, B.; Haesler, J.; Zuber, G.; Hug, W. *Vib. Spectrosc.* **2006**, *42*, 309–316.
(34) Liégeois, V.; Quinet, O.; Champagne, B. *Int. J. Quantum Chem.* **2006**, *106*, 3097–3107.
(35) Lamparska, E.; Liégeois, V.; Quinet, O.; Champagne, B. *ChemPhysChem* **2006**, *7*, 2366–2376.
(36) Liégeois, V.; Champagne, B. *J. Comput. Chem.* **2009**, *30*, 1261–1278.
(37) Jacob, Ch. R.; Reiher, M. *J. Chem. Phys.* **2009**, *130*, 084106.
(38) Jacob, Ch. R.; Luber, S.; Reiher, M. *J. Phys. Chem. B* **2009**, *113*, 6558–6573.
(39) Jacob, Ch. R.; Luber, S.; Reiher, M. *Chem.—Eur. J.* **2009**, *15*, 13491–13508.
(40) Piseri, L.; Zerbi, G. *J. Mol. Spectrosc.* **1968**, *26*, 254–261.
(41) Zerbi, G.; Sandroni, S. *Spectrochim. Acta* **1968**, *24A*, 483–510.
(42) Cui, C. X.; Kertesz, M. *J. Chem. Phys.* **1990**, *93*, 5257–5266.
(43) Cuff, L.; Kertesz, M. *Macromolecules* **1994**, *27*, 762–770.
(44) Kofranek, M.; Kovar, T.; Karpfen, A.; Lischka, H. *J. Chem. Phys.* **1992**, *96*, 4464–4473.
(45) Neugebauer, J.; Reiher, M.; Kind, C.; Hess, B. *J. Comput. Chem.* **2002**, *23*, 895–910.
(46) Buckingham, A. D. *Adv. Chem. Phys.* **1967**, *12*, 107.
(47) Hug, W. *Chem. Phys.* **2001**, *264*, 53–69.
(48) Ahlrichs, R. *TURBOMOLE* V5-10, January 14, 2008; http://www.turbomole.com.
(49) Ahlrichs, R.; Bär, M.; Häser, M.; Horn, H.; Kölmel, C. *Chem. Phys. Lett.* **1989**, *162*, 165–169.
(50) Becke, A. *Phys. Rev. A* **1988**, *38*, 3098–3100.
(51) Perdew, J. P. *Phys. Rev. B* **1986**, *33*, 8822–8824.
(52) Schäfer, A.; Huber, C.; Ahlrichs, R. *J. Chem. Phys.* **1994**, *100*, 5829–5835.
(53) Neugebauer, J.; Herrmann, C.; Luber, S.; Reiher, M. *SNF 4.0: A Program for the Quantum Chemical Calculation of Vibrational Spectra*; http://www.reiher.ethz.ch/software/snf, released February 6, 2007.
(54) Neugebauer, J.; Hess, B. *J. Chem. Phys.* **2003**, *118*, 7215–7225.
(55) Reiher, M.; Brehm, G.; Schneider, S. *J. Phys. Chem. A* **2004**, *108*, 734–742.
(56) Luber, S.; Reiher, M. *Chem. Phys.* **2008**, *346*, 212–223.
(57) Bauernschmitt, R.; Ahlrichs, R. *Chem. Phys. Lett.* **1996**, *256*, 454–464.
(58) Bauernschmitt, R.; Häser, M.; Treutler, O.; Ahlrichs, R. *Chem. Phys. Lett.* **1997**, *264*, 573–578.
(59) Furche, F.; Ahlrichs, R. *J. Chem. Phys.* **2002**, *117*, 7433–7447.
(60) Grimme, S.; Furche, F.; Ahlrichs, R. *Chem. Phys. Lett.* **2002**, *361*, 321–328.
(61) Fedorovsky, M. PyVib2, A Program for Analyzing Vibrational Motion and Vibrational Spectra; 2007; http://pyvib2.sourceforge.net.
(62) Fedorovsky, M. *Comput. Lett.* **2006**, *2*, 233.
(63) Zuber, G.; Hug, W. *J. Phys. Chem. A* **2004**, *108*, 2108.

JP102739G